JOURNAL MEDICAL INFORMATICS TECHNOLOGY
medinftech.org

Segmentation in Identifying the Development of Ground Glass Opacity on CT-Scan Images of the Lungs

Jufriadif Na`am[1*]

[1]*Universitas Nusa Mandiri Jakarta, Indonesia*

ARTICLE HISTORY

Received: 13 March 23
Final Revision: 16 March 23
Accepted: 30 March 23
Online Publication: 31 March 23

KEYWORDS

Ground Glass Opacity (GGO), Computed Tomography Scan (CT-Scan), Segmentation, Identification, Lungs

CORRESPONDING AUTHOR

jufriadifnaam@nusamandiri.ac.id

DOI

10.37034/medinftech.v1i1.1

A B S T R A C T

Ground Glass Opacity (GGO) in the image of the lungs is an object that is white in color. The image was recorded using a Computerized Tomography Scan (CT-Scan). This object has very similar color features to other objects in the lung image, making it very difficult to identify precisely. Likewise by observing the development of this object every time from recording continuously. This study aims to segment the GGO on CT-Scan images that are examined repeatedly due to an increase in complaints against patients. The processed image is an image of the lungs from the CT-Scan equipment. Patients were recorded twice at different time intervals. The processed image is an axial slice of the data cavity as a whole, totaling 12 images for each patient in each recording. The tool used for recording is a CT-Scan with the General Electric (GE) brand model D3162T. The method used is parallel processing with a combination of Image Enhancement techniques, Convert to Binary Image, Morphology Operation, Image Inverted, Active Contour Model, Image Addition, Convert Matrix to Grayscale, Image Filtering, Convert to Binary Image, Image Subtraction and Region Properties. The results of this study can identify the development of the GGO pixel size well, where the increasing number of patient complaints, the larger the GGO area. The extent of development of GGO is irregular with respect to time and examination. Each patient experienced an expansion of GGO by an average of 0.54% to 1.89%. This study is very good and can correctly identify ARF, so it can be used to measure the level of development of ARF in patients with accuracy.

1. Introduction

Ground-Glass Opacity (GGO) is an object of damage to the lungs of people with COVID-19 [1]. This object can be observed in radiological images with Computed Tomography Scan (CT-Scan) or Chest Radiograph (X-Ray) equipment. The image produced by CT-Scan is better than X-Ray because CT-Scan can produce many images while X-Ray is only one image in one recording [2].

GGO is a radiological picture with various etiologies such as inflammation, infection, pulmonary edema, bleeding, pulmonary interstitium. The consequence that can be felt directly is that the function of the lungs is slightly disturbed so that the lungs do not function normally [3], [4]. The characteristic features of GGO have a slightly lighter viscous pattern than normal thoracic tissue [5],[6]. Basically adenocarcinoma of the lung has a size of 3 cm or less than the size of the tumor [7]. It is widely known that GGO has an inadequate prognosis so that it can be considered as early lung cancer [8], [9], [10].

One indication of damage to the thorax due to COVID-19 is the appearance of a Ground-Glass Opacity (GGO) object [11]. In the radiographic image, it can be seen that the GGO object is brighter than the normal chest tissue object because it does not contain air anymore [12]. Several studies published in PubMed, Embase (Elsevier), Google Scholar, and the World Health Organization (WHO) database contained 88% of sufferers who had GGO [13]. As many as 62 patients with pneumonia due to COVID-19 in Wuhan China, 40.3% of the thorax contained GGO [14]. Of the 101 cases of COVID-19 sufferers aged 21-50 years in Hunan China, 86.1% of the thorax contained GGO [15]. Based on this research, there are physiological changes as an observation of the thorax organ for sufferers of COVID-19. This research can be an alternative reference in conducting the initial screening process to make the right decisions in handling COVID-19 sufferers.

2. Research Method

In identifying the GGO pattern on CT-Scan images of COVID-19 sufferers, several stages of the image processing process are carried out. Each stage is interconnected and produces a new image that will be used as input for the next stage. The process stages in this research consist of Dataset, Image Enhancement, Convert to Binary Image, Morphology Operation, Image Inverted, Active Countour Model, Image Addition, Convert Matrix to Grayscale, Image Filtering, Convert to Binary Image, Image Subtraction and Region Properties. All stages of the process are carried out on a Personal Computer (PC) using the Mathlab R2020b Software.

The formulas used in this research are Formula (1), Formula (2), Formula (3), Formula (4), Formula (5), Formula (6), Formula (7), Formula (8), Formula (9), Formula (10), Formula (11), Formula (12), and Formula (13).

$$cl = cl_{\min} + \left[2(\alpha^2) in \left(\frac{1}{1 - DP(f)} \right) \right] \tag{1}$$

$$ag(x,y) = \begin{cases} 0, if \ np(x,y) < NA \\ 1, if \ np(x,y) \geq NA \end{cases} \tag{2}$$

$$CI \circ EP = (CI \Theta EP) \oplus EP \tag{3}$$

$$S(x,y) = L - 1 - R(x,y) \tag{4}$$

$$ac(s) = (k(s), l(s)) \tag{5}$$

$$E_{\text{int}} = E_{elastic} + E_{bend} = a(s)\left|\frac{dv}{ds}\right|^2 + \beta(s)\left|\frac{d^2v}{ds^2}\right|^2 \tag{6}$$

$$E_{elastic} = \int_s a(v(s) - v(s-1))^2 .ds \tag{7}$$

$$E_{bend} = \int_s \beta(v(s-1) - v(s) + v(s+1))^2 .ds \tag{8}$$

$$E^*_{snake} = \int_0^1 E_{snake}(v(s)).ds = \int_0^1 \{E_{\text{int}}(v(s)) + E_{image}(v(s)) + E_{con}(v(s))\}.ds \tag{9}$$

$$CO(x,y) = CI1(x,y) + CI2(x,y) \tag{10}$$

$$GI = \frac{CY - CY_{\min}}{CY_{\max} - CY_{\min}} \tag{11}$$

$$mf(x,y) = median \sum_{(s,t) \in ks_{xy}} cg(s,t) \tag{12}$$

$$CO(x,y) = CI1(x,y) - CI2(x,y) \tag{13}$$

Several articles were used as references in this study [16] – [50].

3. Result and Discussion

In this study, only one test image was presented from 34 images of patients with COVID-19. This input image is 485 x 394 pixel size in JPG format. The patient identities contained in the image are hidden on display in the article to maintain the code of ethics. So that the image presented only includes the chest cavity as the outermost boundar. The results shown in Table 1 .

Table 1. Result Images

Axial	Patient 1		Patient 2	
	1st	2nd	1st	2nd
1	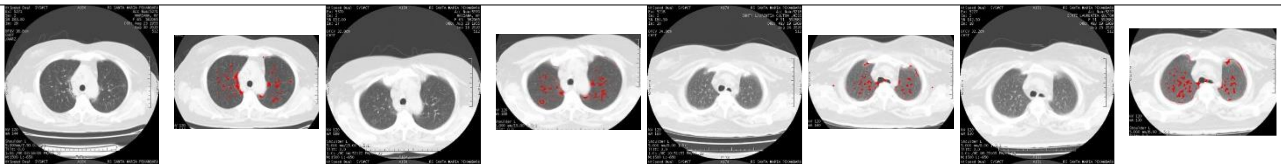			
2	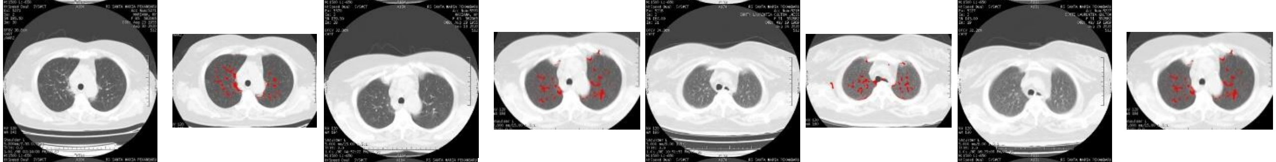			
3	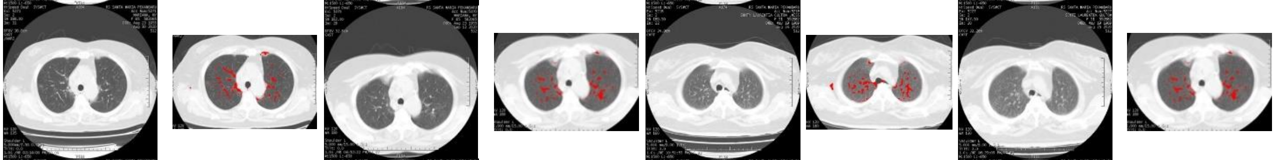			
4	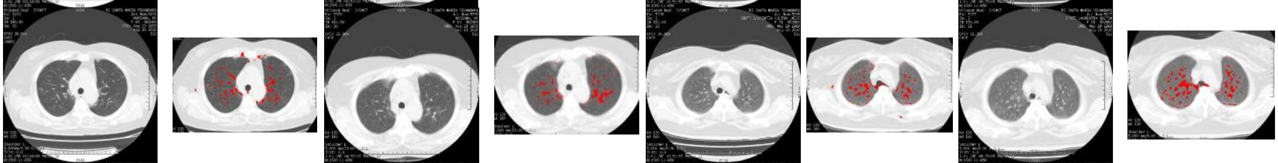			
5	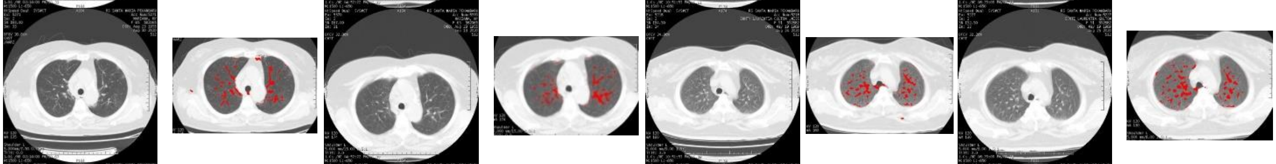			
6	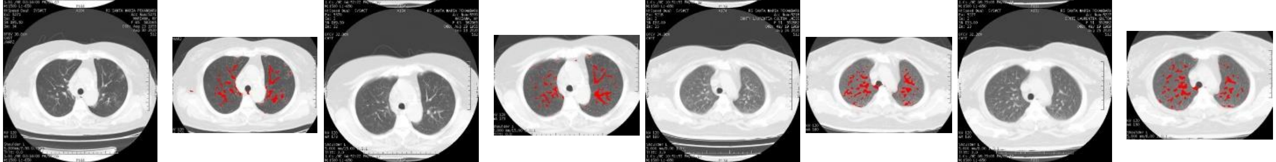			
7	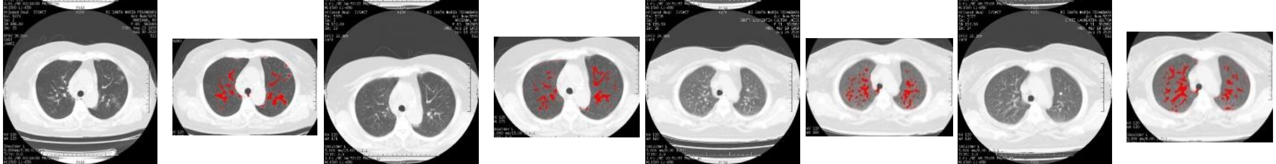			
9	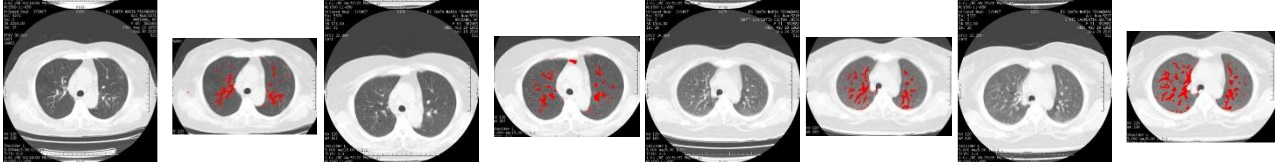			
10	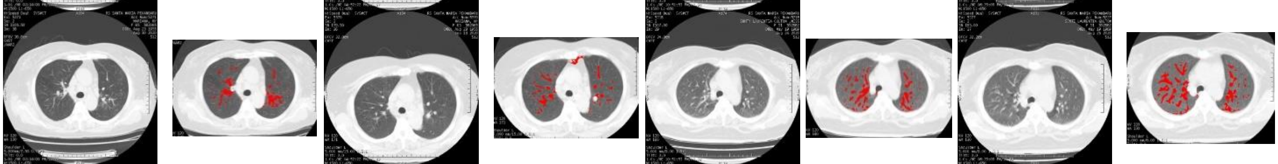			
11	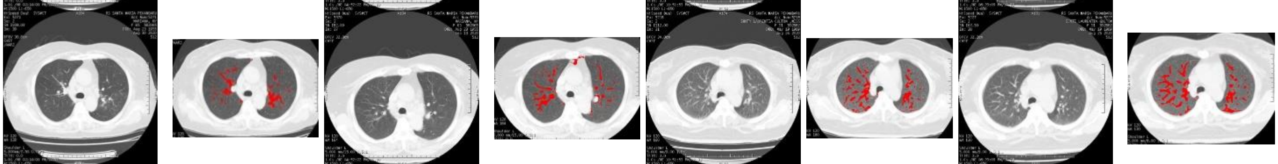			
12	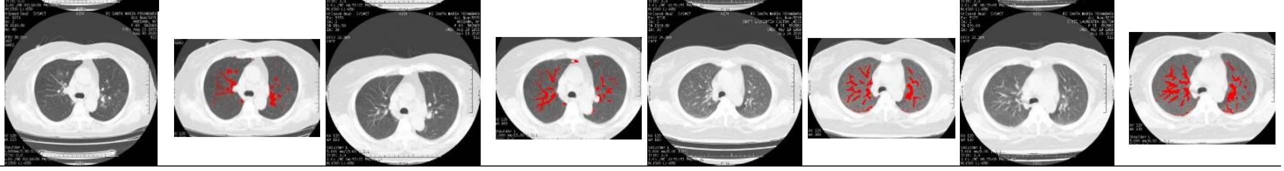			

The objects in the image have been identified very well, so that the pattern from GGO can be recognized. The next step is to count the number of pixels of objects in the image. From the results of this calculation, it can be determined the level of comparison of the area of GGO to the area of the thorax. The calculation used to determine the level of this ratio is the ratio equation presented in Formula (14).

$$Ratio\% = \frac{GGO\ Area}{Thorax\ Area}\ x\ 100\% \qquad (14)$$

Where the ratio is level of the GGO area to the thorax area multiplied by 100%. Based on the results of Formula 14, it can be concluded that the greater the value of the GGO area, the wider the area of the thorax containing GGO. The magnitude of this ratio indicates the higher the severity of patients suffering from Covid-19. The results of calculations for all patients are presented in Table 2.

Table 2. Object Area (Pixel)

No	Patient 1 (W, 65 years old)						Patient 2 (W, 51years old)					
	1st			2nd			1st			2nd		
	Lung	GGO	%	Lung	GGO	%	Lung	GGO	%	Lung	GGO	%
1	17.322	2.024	11,68	14.090	1.968	13,97	10.656	1.572	14,75	14.794	2.676	18,0884
2	17.975	2.010	11,18	15.099	2.495	16,52	11.705	2.121	18,12	15.099	2.495	16,5243
3	18.497	2.365	12,79	16.277	2.582	15,86	12.242	2.686	21,94	16.661	4.010	24,0682
4	19.125	2.819	14,74	17.396	2.820	16,21	12.977	2.710	20,88	17.903	4.276	23,8843
5	19.435	3.216	16,55	18.362	3.224	17,56	13.731	3.168	23,07	19.164	4.291	22,3909
6	19.947	3.426	17,18	19.381	3.668	18,93	14.658	3.760	25,65	20.520	4.292	20,9162
7	20.265	3.302	16,29	20.333	3.624	17,82	15.371	3.525	22,93	20.912	5.146	24,6079
8	20.832	3.474	16,68	21.037	3.656	17,38	16.166	3.999	24,74	20.749	6.277	30,2521
9	20.955	3.385	16,15	21.825	3.643	16,69	17.082	4.216	24,68	21.173	6.563	30,997
10	21.128	3.171	15,01	43.267	3.238	7,48	17.660	4.576	25,91	21.353	6.565	30,7451
11	21.343	3.090	14,48	43.412	3.759	8,66	17.922	4.663	26,02	22.343	6.337	28,3624
12	21.693	3.313	15,27	22.934	3.976	17,34	17.632	4.991	28,31	23.107	6.677	28,896
Sum	238.517	35.595	178,00	273.413	38.653	184	177.802	41.987	277	233.778	59.605	300
Average	19.876,42	2.966,25	14,83	22.784	3.221	15,37	14.817	3.499	23,08	19.481,50	4.967	24,98
Increase						0,54						1,89

The results of image processing presented in Table 2 state that every thorax of a COVID-19 patient has GGO. GGO will result in an increased weakening of the function of the thorax.

4. Conclusion

The results of this study can identify the development of the GGO pixel size well, where the increasing number of patient complaints, the larger the GGO area. The extent of development of GGO is irregular with respect to time and examination. Each patient experienced an expansion of GGO by an average of 0.54% to 1.89%. This study is very good and can correctly identify ARF, so it can be used to measure the level of development of ARF in patients with accuracy.

References

[1] W. Guan et al., “Clinical Characteristics of Coronavirus Disease 2019 in China,” New England Journal of Medicine, vol. 382, no. 18, pp. 1708–1720, Apr. 2020, doi: 10.1056/nejmoa2002032.

[2] W. Herring, *“Learning radiology : recognizing the basics”*, 4th ed, 2-4, 2020. Philadelphia: Elsevier.

[3] L. Chang, Y. Yan, and L. Wang, “Coronavirus Disease 2019: Coronaviruses and Blood Safety,” Transfusion Medicine Reviews, vol. 34, no. 2, pp. 75-80, 2020.

[4] T. Singhal, “A Review of Coronavirus Disease-2019 (COVID-19),” The Indian Journal of Pediatrics, vol. 87, pp. 281–286, 2020.

[5] C.-C. Lai, T.-P. Shih, W.-C. Ko, H.-J. Tang, and P.-R. Hsueh, “Severe acute respiratory syndrome coronavirus 2 (SARS-CoV-2) and corona virus disease-2019 (COVID-19): the epidemic and the challenges,” International Journal of Antimicrobial Agents, vol. 55, no. 3, 2020.

[6] F. A. Rabi, M. S. Al Zoubi, G. A. Kasasbeh, D. M. Salameh, and A. D. Al-Nasser, “SARS-CoV-2 and Coronavirus Disease 2019: What We Know So Far,” Pathogens, vol.9, 2020.

[7] Y. Han, and H. Yang, “The transmission and diagnosis of 2019 novel coronavirus infection disease (COVID-19): A Chinese perspective,” Journal of Medical Virology, vol. 92, no. 6, pp. 639-644, 2020.

[8] D. Wang, B. Hu, C. Hu, et al., “Clinical Characteristics of 138 Hospitalized Patients With 2019 Novel Coronavirus–Infected Pneumonia in Wuhan, China,” Journal of the American Medical Association, vol. 323, no. 11, pp. 1061–1069, 2020.

[9] S. Srivatsan, P. D. Han, K. van Raay, C. R. Wolf, et al., “Preliminary support for a dry swab, extraction free protocol for SARS-CoV-2 testing via RT-qPCR,” bioRxiv, 2020.

[10] S. Ahuja, B. K. Panigrahi, N. Dey, V. Rajinikanth, and T. K. Gandhi, “Deep transfer learning-based automated detection of COVID-19 from lung CT scan slices,” Applied Intelligence, 2020.

[11] M. Chung, A. Bernheim, X. Mei, N. Zhang, M. Huang, X. Zeng, J. Cui, W. Xu, Y. Yang, Z. A. Fayad, A. Jacobi, K. Li, S. Li, and H. Shan, “CT Imaging Features of 2019 Novel Coronavirus (2019-nCoV),” Radiology, vol. 295, no. 1, pp. 202-207, 2020.

[12] A. M. Sirisha and P. Venkateswararao, “Image Processing Techniques on Radiological Images of Human Lungs Effected by COVID-19,” JOIV : International Journal on Informatics Visualization, vol. 4, no. 2, pp. 69, 2020.

[13] W. Guan, Z. Ni, Y. Hu, W. Liang, et al., ”Clinical Characteristics of Coronavirus Disease 2019 in China,” The New England Journal of Medicine, vol. 382, pp. 1708-1720, 2020.

[14] W. Herring. “Learning radiology : recognizing the basics,” 4th ed., Philadelphia: Elsevier. pp. 2–4, 2020.

[15] S. Salehi, A. Abedi, S. Balakrishnan, and A. Gholamrezanezhad, “Coronavirus Disease 2019 (COVID-19): A Systematic Review of Imaging Findings in 919 Patients,” American Journal of Roentgenology, vol. 215, no. 1, pp. 87-93, 2020.

[16] S. Zhou, Y. Wang, T. Zhu, and L. Xia, “CT Features of Coronavirus Disease 2019 (COVID-19) Pneumonia in 62 Patients in Wuhan, China,” American Journal of Roentgenology, vol. 214, no. 6, pp. 1287-1294, 2020.

[17] W. Zhao, Z. Zhong, X. Xie, Q. Yu, and J. Liu, “Relation Between Chest CT Findings and Clinical Conditions of Coronavirus Disease (COVID-19) Pneumonia: A Multicenter Study,” American Journal of Roentgenology, vol. 214, no. 5, pp. 1072-1077, 2020.

[18] V. Rajinikanth, N, Dey, A. N. J. Raj, A. E. Hassanien, K. C. Santosh, and N. S. M. Raja, “Harmony-Search and Otsu based System for Coronavirus Disease (COVID-19) Detection using Lung CT Scan Images,” arXiv, 2020.

[19] D. P. Fan, T. Zhou, G. P. Ji, Y. Zhou, G. Chen, H. Fu, J. Shen, and L. Shao, “Inf-Net: Automatic COVID-19 Lung Infection Segmentation from CT Images,” arXiv, 2020.

[20] D. Das, K. C. Santosh, and U. Pal, “Truncated inception net: COVID-19 outbreak screening using chest X-rays,” Physical and Engineering Sciences in Medicine, vol. 43, pp. 915–925, 2020.

[21] T. Ozturk, M. Talo, E. A. Yildirim, U. B. Baloglu, O. Yildirim, and U. R. Acharya, “Automated detection of COVID-19 cases using deep neural networks with X-ray images,” Computers in Biology and Medicine, vol. 121, 2020.

[22] S. Minaee, R. Kafieh, M. Sonka, S. Yazdani, and G. J. Soufi, “Deep-COVID: Predicting COVID-19 from chest X-ray images using deep transfer learning,” Medical Image Analysis, vol. 65, 2020.

[23] I. D. Apostolopoulos, and T. A. Mpesiana, “Covid-19: automatic detection from X-ray images utilizing transfer learning,” Physical and Engineering Sciences in Medicine, vol. 43, pp. 635-640, 2020.

[24] A. Narin, C. Kaya, and Z. Pamuk, “Automatic Detection of Coronavirus Disease (COVID-19) Using X-ray Images and Deep Convolutional Neural Networks,” arXiv, 2020.

[25] G. Siracusano, A. L. Corte, M. Gaeta, G. Cicero, M. Chiappini, and G. Finocchio, “Pipeline for Advanced Contrast Enhancement (PACE) of chest X-ray in evaluating COVID-19 patients by combining bidimensional empirical mode decomposition and CLAHE,” Sustainability, vol. 12, 2020.

[26] M. Loey, G. Manogaran, and N. E. M. Khalifa, “A deep transfer learning model with classical data augmentation and CGAN to detect COVID-19 from chest CT radiography digital images,” Neural Computing and Applications, 2020.

[27] D. Singh, V. Kumar, Vaishali and M. Kaur, “Classification of COVID-19 patients from chest CT images using multi-objective differential evolution–based convolutional neural networks,” European Journal of Clinical Microbiology & Infectious Diseases, 2020.

[28] Y. Yunus, J. Harlan, J. Santony, R. Hidayat, and J. Naam, “Enhancement on Enlarge Image for Identification Lumbar Radiculopathy at Magnetic Resonance Imaging,” TEM Journal, vol. 9, no. 2, pp. 649-655, 2020.

[29] S. M. Pizer, E. P. Amburn, J. D. Austin, R. Cromartie, A. Geselowitz, et al., “Adaptive histogram equalization and its variations, Computer Vision, Graphics, and Image Processing,” Computer Vision, Graphics and Image Processing, vol. 39, pp. 355–68, 1987.

[30] Sonali, S. Sahu, A. K. Singh, S. P. Ghrera, M. Elhoseny, “An approach for de-noising and contrast enhancement of retinal fundus image using CLAHE,” Optics & Laser Technology, vol. 110, pp. 87-98, 2019.

[31] W. N. J. H. W. Yussof, M. S. Hitam, E. A. Awalludin, and Z. Bachok, “Performing contrast limited adaptive histogram equalization technique on combined color models for underwater image enhancement,” International Journal of Interactive Digital Media, vol. 1, no. 1, pp. 1-6, 2013.

[32] D. J. Hemanth, O. Deperlioglu and U. Kose, “An enhanced diabetic retinopathy detection and classification approach using deep convolutional neural network,” Neural Computing and Applications, vol. 2, no. 3, pp. 707-721, 2020.

[33] P. Parida, and R. Rout, “Transition region based approach for skin lesion segmentation,” ELCVIA: Electronic Letters on Computer Vision and Image Analysis, vol. 19, no. 1, pp. 28-37, 2020.

[34] G. K. Chadha, A. Srivastava, A. Singh, R. Gupta, and D. Singla, “An Automated Method for Counting Red Blood Cells using Image Processing,” Procedia Computer Science, vol. 167, pp. 769-778, 2020.

[35] E. Murali, and K. Meena, “Brain Tumor Detection from MRI using Adaptive Thresholding and Histogram based Techniques,” Scalable Computing: Practice and Experience, vol. 21, no. 1, pp. 3-10, 2020.

[36] A. Ledda, “Mathematical Morphology in Image Processing,” Doctoral dissertation, PhD thesis, Ghent University, Ghent, Belgium, 2007.

[37] R. M. Haralick, S. R. Sternberg, and X. Zhuang, “Image analysis using mathematical morphology,” IEEE Transactions on Pattern Analysis and Machine Intelligence, vol. 4, pp. 532-550, 1987.

[38] J. Serra, Image Analysis and Mathematical Morphology, London: Academic Press, 1982.

[39] B. Li, and S. T. Acton, “Active contour external force using vector field convolution for image segmentation,” IEEE Transactions on Image Processing, vol. 16, no. 8, pp. 2096-2106, 2007.

[40] R. Ronfard, “Region-based strategies for active contour models,” International Journal of Computer Vision, vol. 13, no. 2, pp. 229-251, 1994.

[41] M. Kass, A. Witkin, and D. Terzopoulos, “Snakes: Active contour models,” International Journal of Computer Vision, vol. 1, no. 4, pp. 321-331, 1988.

[42] R. C. Gonzalez, and R. E. Woods, Digital image processing, Upper Saddle River, New Jersey: Prentice Hall, 2002.

[43] Y. Zhang, J. Qian, O. Zaltzhendler, et al., “Analysis of in vivo uterine peristalsis in the non-pregnant female mouse,” Interface Focus, vol. 9, no. 4, 2019.

[44] L. Novamizanti, A. L. Prasasti, and I. F. N. Kiranda, “Comparison of discrete cosine transform and dual-tree complex wavelet transform based on arithmetic coding in medical image compression,” In Journal of Physics: Conference Series, 2020, vol. 1367, no. 1, p. 012021.

[45] Y. Zhu,, and C. Huang, “An improved median filtering algorithm for image noise reduction,” Physics Procedia, vol. 25, pp. 609-616, 2012.

[46] M. P. Sukassini, and T. Velmurugan, “Noise removal using morphology and median filter methods in mammogram images,” In The 3rd International Conference on Small and Medium Business, 2016, pp. 413-419.

[47] A. A. Sheikh, M. S. Azmi, M. A. Aziz, M. N. Al-Mhiqani, and S. S. Bafjaish, “Diacritic segmentation technique for arabic handwritten using region-based,” Indonesian Journal of Electrical Engineering and Computer Science, vol. 18, no. 1, pp. 478-484, 2020.

[48] J. Ananthanarasimhan, P. Leelesh, M. S. Anand, and R. Lakshminarayana, “Validation of projected length of the rotating gliding arc plasma using ‘regionprops’ function,” Plasma Research Express, vol. 2, no. 3, 2020.

[49] N. J. Shoumy, P. Ehkan, S. N. Yaakob, M. S. Ali, and S. Khatun, “Feature extraction for neural network pattern recognition for bloodstain analysis,” International Journal of Applied Engineering Research, vol. 11, no. 15, pp. 8583-8589, 2016.

[50] F. S. Pranata, J. Naam, and R. Hidayat, “Color Feature Segmentation Image for Identification of Cotton Wool Spots on Diabetic Retinopathy Fundus,” International Journal on Advanced Science, Engineering and Information Technology, vol. 10, no. 3, pp. 974-979, 2020.